N/S Co-doped Free-standing Carbon Electrode Derived from Waste Facial Masks for Anti-freezing Flexible Quasi-solid-state Supercapacitors

Yong Ye, Hongchuan Zhang, Yu Shi, Yijang Liu, Huaming Li, Zhiyu Wang, Mei Yang and Bei Liu

Experimental

Materials

The waste facial masks (PROYA, Proya Cosmetics Co., Ltd) was collected from Xiangtan University campus. Dimethyldithiocarbamic acid sodium ($C_3H_6NNaS_2 \cdot 2H_2O$, denoted as DTC, 92 wt%), hydrochloric acid (HCl) and anhydrous ethanol (C_2H_5OH) were purchased from Shanghai Energy-chemical Reagent Co., Ltd. Besides, polyethyleneimine (PEI, 99 %), lithium bis (trifluoromethyl sulfonyl) imide (LiTFSI), formaldehyde (CH_2O), glyoxal ($C_2H_2O_2$), acetic acid (CH_3COOH) and 1-ethyl-3-methylimidazolium bis (trifluoromethyl sulfonyl) imide (EMIMTFSI) were purchased from Shanghai Macleans Biochemical Co., Ltd. All chemical reagents were analytical grade and used as received without further purification.

Synthesize of NSCC electrodes.

Waste facial masks were cut into identical pieces with a size of 2 × 5 cm. Prior to usage, the remaining contaminants in the recycled masks have been purged by thoroughly washing in boiling water followed by ultrasound treatment in ethanol. Subsequently, the facial mask fabrics (FMFs) were immersed in an aqueous solution of dimethyldithio carbamic acid sodium (DTC) with various concentrations (0.5, 1, 1.5, 2, 2.5 M) under stirring at 80°C for 8 h. After filtration, the products were

pyrolyzed in N$_2$ flow for 2 h at different temperatures (600, 700 and 800 °C) at a ramp rate of 5°C min^{-1}. The resulting samples were then washed with diluted HCl solution and DI water until neutral to yield NSCC electrodes. For comparison, the facial mask fabric pieces without DTC treatment (denoted as CC) were also produced similarly.

Synthesize of MPEI-TF-IL gel electrolyte

The MPEI-TF-IL gel electrolyte was synthesized according to our previous work.[1] The polyethyleneimine (PEI, 5.64 mmol) was dissolved in DI water (15 mL), followed by adding glyoxal (1.44 mL, 16.9 mmol), formaldehyde (0.98 mL, 16.9 mmol) and acetic acid (4.85 mL, 28.2 mmol) at 0 °C. After stirring for 30 minutes, the solution was heated at 60 °C under stirring for 24 h. After cooling to room temperature, lithium bis(trifluoromethanesulfonyl)imide (LiTFSI)(1.0 M, 200 mL) was added into this mixture solution under stirring for 12 h for anion exchange. The resulting imidazolium TFSI-cross-linked PEI (denoted as MPEI-TF) was dialyzed against DI water for 12 h to remove excess LiTFSI. The water-swollen MPEI-TF with 50% water (0.50 g) was finally mixed with EMIMTFSI (1.0 g) with a mass ratio of 1 : 4 (denoted as MPEI-TF-IL). After freeze-drying, MPEI-TF-IL (0.5 g) was reswollen in anhydrous acetone (10 mL) under stirring for 2 h.

Material Characterization.

Scanning electron microscopy (SEM) and Energy dispersive spectroscopy (EDS, Hitachi, SU8010) were performed to investigate the morphology of the composite materials. The elemental analysis was performed by X-ray photoelectron spectroscopy (XPS, Thermo Fisher, Nexsa). Fourier transform infrared spectra (FT-IR, Thermo Nicolet 6700 spectrometer) was used to characterize the surface properties of all samples. Auto tensile tester (AG-X plus, Shimadzu, Kyoto, Japan) was used to characterize the mechanical properties of the samples. The wettability was determined by Contact angles measurement (LAUDA Scientific GmbH, LSA-100). ASAP-2020 surface analyzer (Micromeritics instrument Ltd., USA, 77 K) was used to obtain nitrogen adsorption isotherms.

Electrochemical measurements

Cyclic voltammetry (CV), electrochemical impedance spectroscopy (EIS) and Galvanostatic charge-discharge (GCD) analysis were performed on CHI 760E

electrochemical workstation. For three-electrode tests. The NSCCs electrodes with a size of 1 × 1.5 cm (2 mg cm^{-2}) were directly used as the working electrodes. The operative measurement region spanned 1 × 1 cm, accounting for *ca.* 2.0 mg of active mass. A platinum foil and Hg/HgO electrode were used as the countered and reference electrode, respectively. The electrolyte is 6 M KOH. The FQSC was assembled by using two pieces of NSCC-700 with a size of 1 × 4 cm (2 mg cm^{-2}) as the working electrodes in MPEI-TF-IL gel polymer electrolyte. The operative measurement region spanned 1× 2 cm.

The specific capacitance, capacitance contribution, specific energy and power were calculated by the following Equations:

$$C_g = I / (m dv/d_t) \tag{1}$$

$$C_s = 2I / (m dv/d_t) \tag{2}$$

$$i = k_1 v + k_2 v^{1/2} \tag{3}$$

$$i = a^v b \tag{4}$$

$$E = C_s \Delta V^2 / (8 \times 3.6) \tag{5}$$

$$P = 3600 \times E / \Delta t \tag{6}$$

where C_g and C_s (F g^{-1}) is the specific capacitance measured three and two-electrode system, respectively. I (A) is the current, m (g) is the mass of the measurement area of electrode, dv/d_t (V s^{-1}) is the slope of the discharge curve, $k_1 v$ stands for electrical double-layer capacitance (EDLC) and $k_2 v^{1/2}$ represents pseudocapacitance, ΔV denotes the voltage change excluding the *IR* drop during the discharge process, E (W h kg^{-1}) and P (W kg^{-1}) represents specific energy and power, respectively.
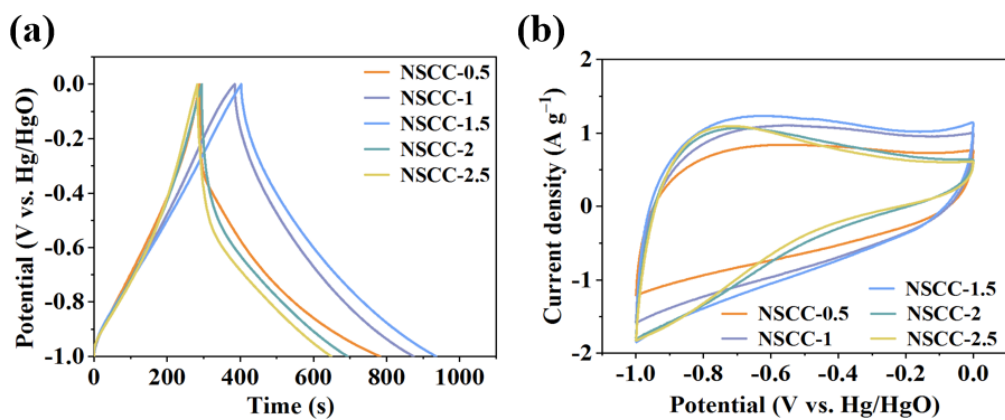
Fig. S1 (a) GCD curves at a current density of 0.5 A g^{-1} and (b) CV curves at a scan rate of 5 mV s^{-1} for NSCC electrodes prepared with different DTC concertations ranging from 0.5 to 2.5 M.
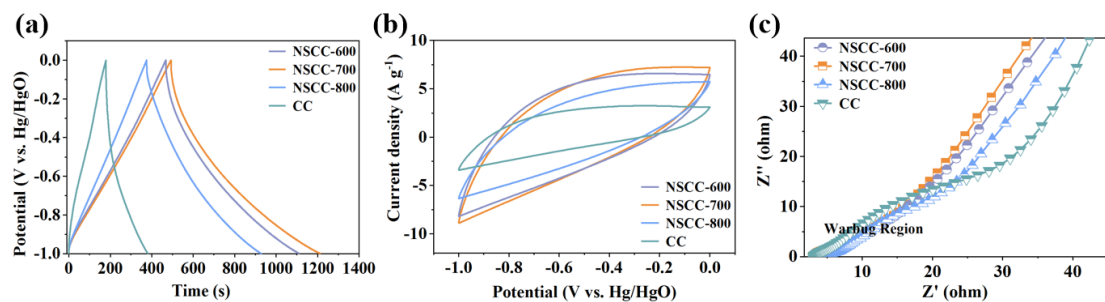
Fig. S2 (a) GCD curves at a current density of 0.5 A g^{-1}, (b) CV curves at a scan rate of 5 mV s^{-1} and (c) Nyquist plots for NSCC electrodes prepared with 1.5 M DTC at various temperatures ranging from 600 to 800 ^{o}C.
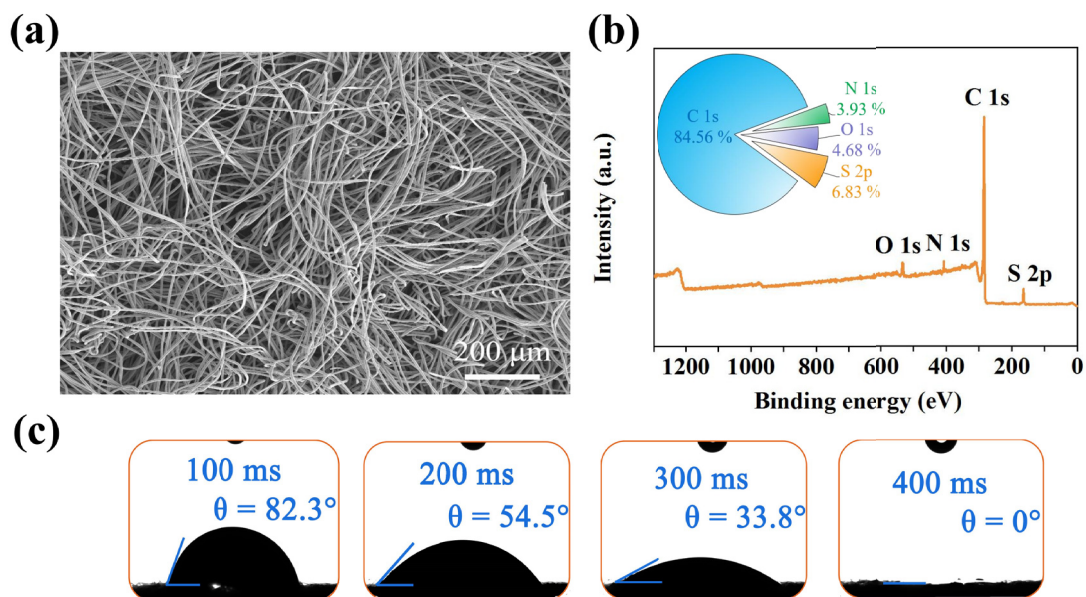
Fig. S3 (a) SEM image, (b) XPS survey scan and (c) contact angle tests of NSCC-700.
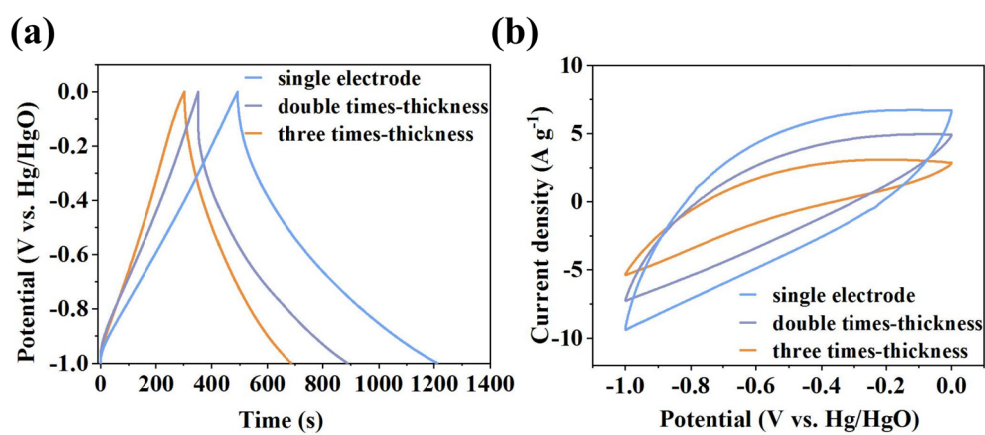
Fig. S4 (a) GCD curves at a current density of 0.5 A g^{-1} and (b) CV curves at a scan rate of 5 mV s^{-1} for NSCC-700 electrodes with different times-thickness.
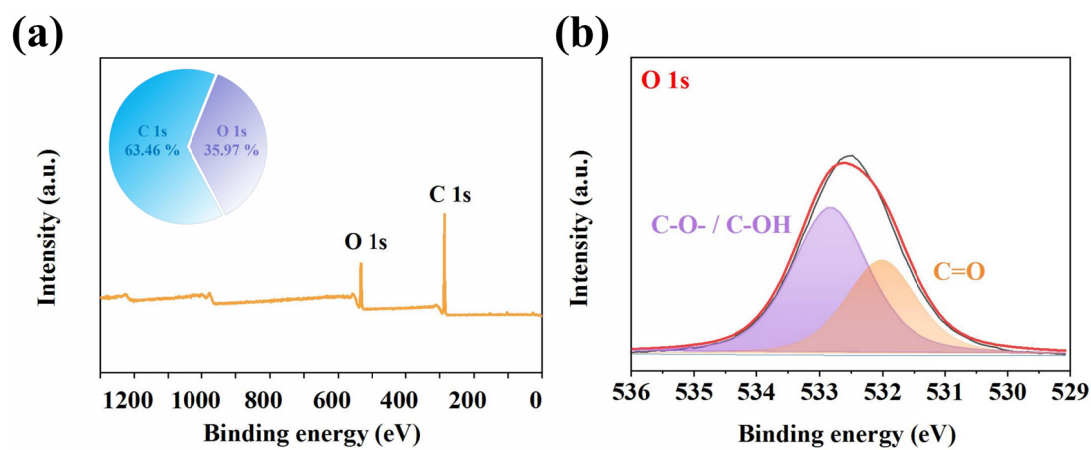
Fig. S5 (a) XPS survey scan and (b) high-resolution O 1s XPS spectrum for facial mask fabric (FMF).
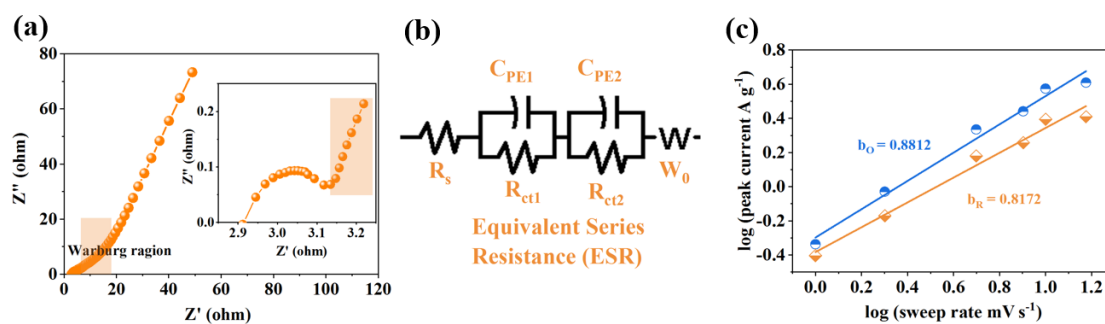
Fig. S6 (a) Nyquist plots of NSCC-700. (b) The equivalent circuit model used for fitting the EIS data. (c) Linear relationship between log (*peak current*) and log(*sweep rate*).
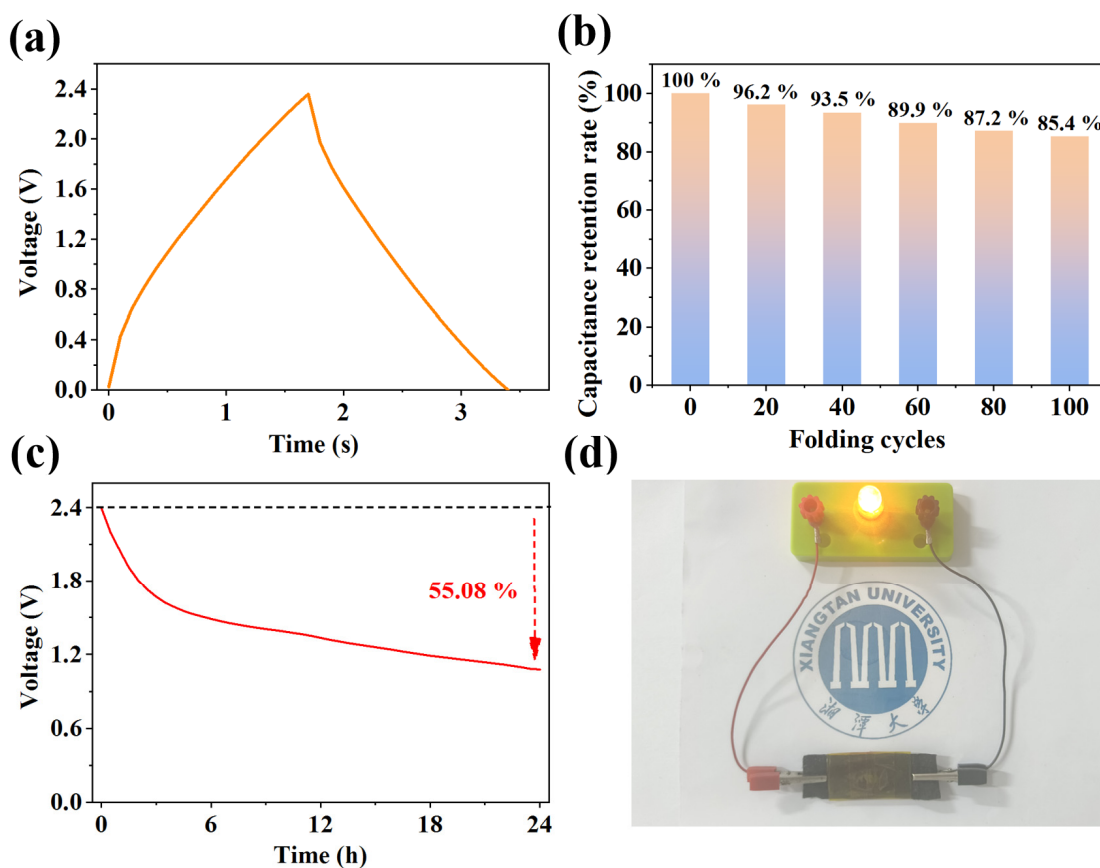
Fig. S7 (a) GCD profile at 25 °C at a current density of 20 A g^{-1}. (b) Capacitance retention against folding cycles, (c) the self-discharge curve and (d) the photographic image of a LED powered by the NSCC-700 FQSC.
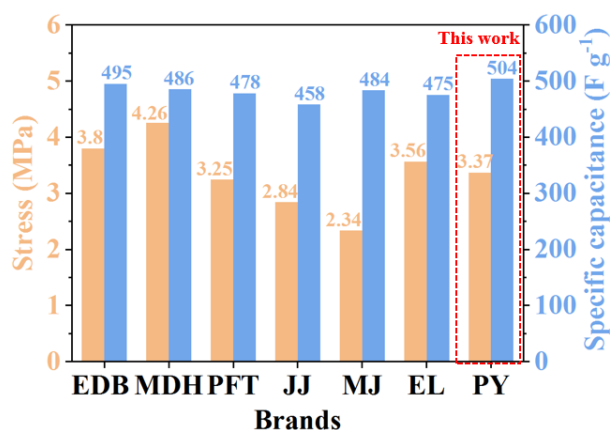
Fig. S8 The tensile strength of various brands of FMFs and specific capacitance of NSCC electrodes derived from various brands of FMFs.

Table S1 Textural properties of NSCC-700.

BET SSA ($m^2\,g^{-1}$)		Pore volume ($cm^3\,g^{-1}$)		Pore size (nm)
Total	Micro	Total	Micro	Average
316.46	254.51	0.17	0.13	2.21

Table S2 A comparison of NSCC-700 with reported free-standing carbon electrodes in specific capacitance.

Electrode	Precursor	Electrolyte	Current density	Capacitance (C_g, F g^{-1})	Ref.
ACNT/WC	Fir wood	6 M KOH	1 mA cm^{-2}	493.7	S2
CA-CNFs-800	CA nanofiber membrane	6 M KOH	0.2 A g^{-1}	229.4	S3
C-800	Kraft lignin	1 M H_2SO_4	1 A g^{-1}	196.6	S4
a-C/CP-160-4	Cellulose carbon fibers	6 M KOH	0.5 A g^{-1}	275.6	S5
FHNC-2	Carbon foam	6 M KOH	1 A g^{-1}	280.3	S6
ACFP-15	Carbon fiber papers	6 M KOH	0.1 mA cm^{-2}	165	S7
HPCF-10	Carbon fibers	3 M KOH	1 A g^{-1}	283	S8
PLC-650-2	Lignin	6 M KOH	1 A g^{-1}	320	S9
M-CMA-800	Wood	1 M KOH	0.5 A g^{-1}	408.5	S10
CNF papers	Carbon nanofiber papers	6 M KOH	10 mV s^{-1}	272	S11
SNC-800	Polyethersulfone	6 M KOH	1 A g^{-1}	240	S12
G-CDP-900	Poplar	1 M KOH	1 A g^{-1}	189	S13
NSCC-700	**Waste facial mask**	**6 M KOH**	**0.2 A g^{-1}**	**504**	**This**
			1 A g^{-1}	**385**	**work**

Table S3 A comparison of NSCC-700 FQSC with reported ones in energy density (E), power density (P) and cycling stability.

Electrodes	Voltage (V)	Electrolyte	Capacitance (C_s, F g^{-1})	E_{max} (Wh kg^{-1})	P_{max} (kW kg^{-1})	Cycling stability	Ref.
CA-CNFs-800	0–1	KOH	116.6 (0.5 A g^{-1})	16.4	16.1	97.3 % (40,000)	S3
C-800	0–1.6	H$_2$SO$_4$	114.88 (1 A g^{-1})	62.6	1.25	99.5 % (10,000)	S4
a-C/CP-160-4	0–1	PVA-KOH	126.5 (0.5 A g^{-1})	17.5	12.3	87 % (20,000)	S5
HPCF-10	0–1.5	KOH	353 (1 A g^{-1})	17.8	29.7	90.5 % (10,000)	S8
CNF papers	-1.1–0	KOH	142 (5 mV s^{-1})	5.66	2.75	94 % (10,000)	S11
G-CDP-900	0–1.4	KOH	43 (0.25 A g^{-1})	11.6	3.5	70 % (10,000)	S13
PCFL-33	0–1.3	H$_2$SO$_4$	48 (0.5 A g^{-1})	8.4	47	85 % (5,000)	S14
AC/lig-MnO$_2$	1–2	PVA-H$_3$P$_4$	5.52 mF cm^{-2} (6.01 mA g^{-1})	14.1	1	97.5 % (2,000)	S15
NSCC-700	**0–2.4**	**MFSI-TF-IL (25 °C)**	**149 (0.1 A g^{-1})**	**29.85**	**20.83**	**88.6 % (5,000)**	**This work**
		MFSI-TF-IL (-20 °C)	**115 (0.1 A g^{-1})**	**20.43**	**16.72**	**–**	

Table S4 Physical properties of various brands of facial mask fabrics (FMFs) used in our work.

Brands of FMFs	Areal density (g m⁻²)	Thickness (mm)	Contact angle	Average Pore size (mm)	Porosity (%)
EVIDENS DE BEAUTE (EDB)	31.2	0.29	32.6°	45.25	92.20
MEDIHEAL (MDH)	53.7	0.31	48.2°	41.58	88.45
PERFECTACE (PFT)	42.4	0.30	37.6°	45.68	87.45
JAYJUN (JJ)	22.8	0.23	35.6°	55.57	89.05
Montagne Jeunesse (MJ)	22.3	0.23	37.2°	47.52	92.42
Estee Lauder (EL)	40.8	0.29	45.6°	41.38	91.83
PROYA **(PY, this work)**	**38.4**	**0.33**	**42.6°**	**36.45**	**89.52**

References

1   S. Y. Yu, B. Liu, M. Yang, H. B. Chen, Y. J. Liu and H. M. Li, *ACS Sustain. Chem. Eng.*, 2022, **10**, 5548-5558.

2   M. J. Zeng, X. F. Li, W. L, T. Y. Zhao, J. Wu, S. M. Hao and Z. Z. Yu, *Appl. Surf. Sci.*, 2022, **598**, 153765.

3   Y. L. Wang, J. X. Cui, Q. L. Qu, W. J. Ma, F. H. Li, W. H. Du, K. M. Liu, Q. Zhang, S. J. He and C. B. Huang, *Micropor. Mesopor. Mater.*, 2022, **329**, 111545.

4   M. Singh, A. Gupta, S. Sundriyal, K. Jain and S. R. Dhakate, *Mater. Chem. Phys.*, 2021, **264**, 124454.

5   B. Y, L. Feng, J. J. Zheng, Q. Zhang, Y. Z. Dong, Y. C. Ding, W. S. Yang, J. Q. Han, S. H. Jiang and S. J. He, *Appl. Surf. Sci.*, 2023, **608**, 155144.

6   Y. Z. Wang, Y. X. Liu, D. H. Wang, C. Wang, L. Guo and T. F. Yi, *Appl. Surf. Sci.*, 2020, **506**, 145014.

7   J. J Chen, J. X. Xie, C. Q. Jia, C. Y. Song, J. Hu and H. L. Li, *Chem. Eng. J.*, 2022, **450(1)**, 137938.

8   C. Y. Liu, L. Wang, Z. P. Xia, R. X. Chen, H. L. Wang and Y. Liu, *Chem. Eng. J.*, 2022, **431(2)**, 134099.

9   F. B. Fu, D. J. Yang, W. L. Zhang, H. Wang and X. Q. Qiu, *Chem. Eng. J.*, 2020, **392**, 123721.

10   H. G. Luo, R. R. Si, C. W. Li, J. L. Zhang, P. Li, Y. B. Tao, X. Zhao, H. L. Chen and J. C. Jiang, *Mater. Chem. Front.*, 2022, **6**, 379-389.

11   T. T. Wang, X. He, W. B. Gong, Z. H. Kou, Y. Yao, S. Fulbright, K. F. Reardon and M. H. Fan, *Fuel Process. Technol.*, 2022, **225**, 107055.

12   Y. Wang, S. Q. Wang, Y. Jin, Y. Liu, J. Luo, S. Q. Nie and D. F. Liu, *Mater. Lett.*, 2022, **325**, 132896.

13   J. L. Zhang, S. H. Jiao, H. G. Luo, M. Gao, C. W. Li, H. X. Zhang, F. G. Kong, X. Zhao, H. L. Chen and J. C. Jiang, *J. Power Sources*, 2023, **562**, 232787.

14   F. J. G. Mateos, R. R. Rosas, J. M. Rosas, E. Morallón, D. C. Amorós, J. R. Mirasol and T. Cordero, *Sep. Purif. Technol.*, 2020, **241**, 116724.

15   S. Jha, S. Mehta, Y. Chen, L. Ma, P. Renner, D. Y. Parkinson and H. Liang, *ACS Sustain. Chem. Eng.*, 2020, **8**, 498-511.